SUPERPIXEL-BASED HYPERSPECTRAL UNMIXING WITH REGIONAL SEGMENTATION

Mohammed Q. Alkhatib[1,2] and Miguel Velez-Reyes[1], Senior Member
[1]The University of Texas at El Paso, El Paso, TX, USA, 79968
[2]Abu Dhabi Polytechnic, Al Ain, AZ, UAE, P.O. Box 66844
mqalkhatib@ieee.org, m.velez@ieee.org

ABSTRACT

In this paper, a superpixel-based hyperspectral image unmixing is proposed. First, superpixel segmentation is applied to the image. A low dimensional representation of the image is created by representing each superpixel by its mean spectra. Second, the superpixel image is segmented into regions. Endmember extraction is applied to each region to extract local endmembers. Abundances are computed over the full image using the extracted endmembers. The approach is compared with the global unmixing and the local unmixing using the original image. Experimental results are presented using the HYDICE Urban hyperspectral image.

Index Terms— Hyperspectral unmixing; Superpixel segmentation; Column subset selection.

1 INTRODUCTION

In hyperspectral imaging, the measured pixel spectral signature is the mixing of the materials in the field of view of the sensor. The linear unmixing problem refers to finding the number of endmembers, their spectral signatures, and their abundances (or fractional area coverage) from a given hyperspectral image. Multiple approaches are described in the literature for unmixing [1].

Superpixels incorporate spatial connectivity to group similar pixels in a spatial neighborhood. If a pixel and its neighbors are similar, they can be treated as a single entity in subsequent processing. Therefore, superpixels can result in reduced computational requirements for the image processing task, since processing is performed in the reduced set of superpixels and results are interpolated to the original image pixels. A lower dimensional representation of the image can be obtained by representing each superpixel by its mean spectral signature. This averaging has a denoising effect, which another important advantage of superpixel representation. Superpixel-based representation have shown to be successful in improving the performance of hyperspectral unmixing and noise reduction [2, 3].

Most unmixing techniques do not consider spatial information [4]. The degree to which spatial information is relevant to the unmixing process is strongly correlated with the spatial resolution and the scale of the features on the ground surface being imaged. Image segmentation has shown to be a useful approach for endmember extraction to capture endmember spectral variability across the scene and capture small endmembers that can be missed by global approaches [5]. Here we combine superpixel-based unmixing and segmentation in unmixing.

The paper is organized as follows. Section 2 presents the proposed approach. Section 3 presents experimental results. Section 4 presents conclusions and final remarks

2 SUMMARY OF METHOD

The proposed approach is depicted in Fig. 1. A brief summary of each component is given next.

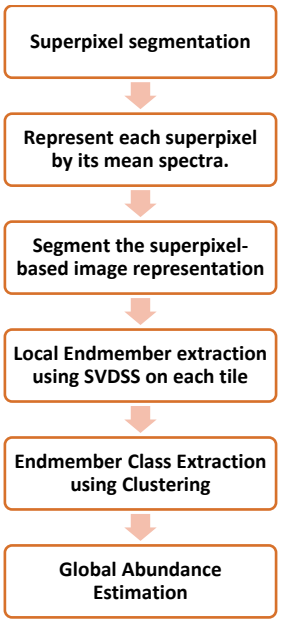

Fig. 1 Proposed superpixel-based unmixing.

2.1 Superpixel Image Segmentation using SLIC

The value of the superpixel representation in image processing and computer vision has been recognized in the literature. Simple linear iterative clustering (SLIC) [6] algorithm showed better performance in superpixel segmentation than other methods in terms of computation speed and memory efficiency [6]. Here SLIC is used for superpixel segmentation in the proposed unmixing method.

The Simple Linear Iterative Clustering (SLIC) is a simple method to decompose an image into homogenous regions. It is based on a spatially localized version of the k-means clustering.

SLIC starts by dividing the image into an equally spaced grid. The center of each grid tile is then used to initialize a corresponding k-means clustering. After k-means, SLIC

optionally removes any segment whose area is smaller than a predefined threshold by merging them into larger superpixels. The details of the algorithm are described in [6].

2.2 Low Dimensional Representation using Superpixel Mean Spectra

In this step, each SLIC superpixel is represented by the mean spectra of the spectral signatures in the superpixel. This result in a lower dimensional (LD) representation corresponding to a non-uniform spatial sampling of the image.

2.3 Quad-tree Segmentation of the LD mean image

As shown in [7], quadtree segmentation helps in capturing spatially local endmembers that are lost in global endmember extraction and help captures endmember spectral variability across a scene. In the example presented here, we only needed to partition the LD-SLIC image in four quadrants.

2.4 Endmember Extraction

Endmember extraction will be performed on each quadrant using the Singular Value Decomposition Subset Select (SVDSS) of [8]. SVDSS is an algorithm used to select the most independent subset of columns from a matrix. It has been applied to band subset selection in the past [8].

The number of endmembers is determined using the gram matrix method described in [9]. The determinant (or Gramian) of the Gram Matrix is the square of the volume of the parallelepiped formed by the vectors [9]. Here the Gramian is computed for the set of endmembers starting with three and increased until the Gramian approaches zero. The endmembers are ordered by decreasing magnitude such that the convex hull volume generally reaches a peak at a small number of endmembers and is then a monotonically decreasing function.

2.5 Endmember Classes

Regional (or per segment) endmembers are combined into *endmember classes* using clustering techniques. In the experiments presented later, endmembers were clustered using cosine distance as a similarity measure.

2.6 Abundance Estimation

Spectral endmember abundances are computed by solving the constrained linear least squares problem [10]:

$$\hat{\mathbf{a}}_i = \arg \min_{a_{ij} \geq 0, \sum_{j=1}^{p} a_{ij} \leq 1} \left\| \mathbf{x}_i - \bar{\mathbf{S}} \mathbf{a}_i \right\|_2^2 \qquad (1)$$

where $\mathbf{x}_i$ the measured spectral signature for the *i-th* pixel, $\mathbf{a}_i$ is the corresponding abundance vector, and $\bar{\mathbf{S}}$ is the endmember matrix that includes all extracted spectral endmember signatures from all tiles in the image. The abundances satisfy positivity and sum less than or equal to one (SLO) constraint. The reason for using SLO constraint instead of the sum-to-one (STO) constraint is to account for topography effects as described in [10].

The abundance of an endmember class is the sum of the abundances of the spectral endmembers in it.

3 Experimental Results

Next, experimental results show the improvement provided by the proposed approach.

3.1 Hyperspectral Data

The image used in this paper is the HYDICE Urban scene [11]. The image is a 307 x 307 pixels scene at 2 m resolution, with 210 bands ranging from 400 nm to 2500 nm at 10 nm resolution. Channels 1--4, 76, 87, 101--111, 136--153 and 198--210 are removed (due to dense water vapor and atmospheric effects) leaving 162 bands used in the analysis. Fig. 2(a) shows a true color composite of the scene. There are 5 classes in the scene as shown in Fig 2(b).

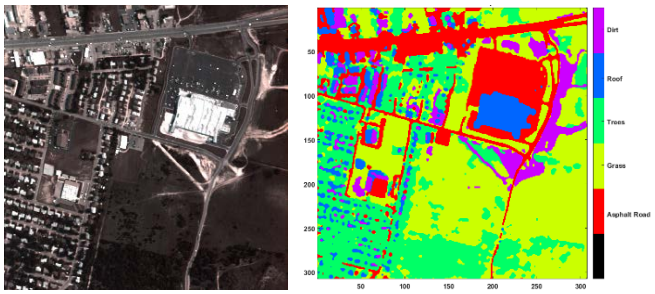

Fig.2. Urban Image: (a) true color RGB composite; (b) Reference data classification map [11].

3.2 Segmentation Results

Fig. 3 shows the SLIC superpixel segmentation with a region size of 16 pixels, which kept spatial features of interest and resulted in a 20x20 grid of superpixels.

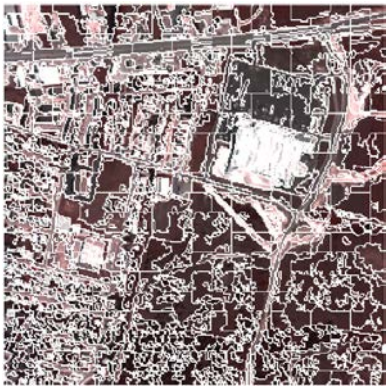

Fig.3. SLIC image of the urban scene.

Each superpixel is presented by its mean spectra which results in a low dimensional (LD) non-uniform grid representation of 20x20 pixels. The mean image is segmented into 4 quadrants before proceeding into the endmember extraction step.

3.3 Endmember Extraction

The number of spectral endmembers in each quadrant estimated using the gram method are shown in Table 1. A total of 31 spectral endmembers were extracted using SVDSS applied to each quadrant. The extracted spectral endmembers

were clustered using the cosine distance with a threshold of 99.5%. Clustering analysis resulted in 19 endmember classes. The endmember classes are manually grouped to form information classes commensurate with the reference map.

Table 1: Estimated Number of Endmembers on Each Image Quadrant.

Quadrant	# of SEM	Quadrant	# of SEM
Upper left	8	Upper right	9
Lower left	7	Lower right	7

3.4 Abundance Estimates and Classification

Abundances were computed by solving (1) using the NNSLO algorithm described in [10]. Endmembers and abundance maps are shown in Fig. 4. Classification maps are generated using winner takes it all approach with a 50% threshold. If the winner does not have 50% or more abundance, the pixel is not classified. Quantitative analysis is based on overall accuracy, kappa statistic, user's and producer's accuracies for each map. We compare the proposed approach with global analysis using all pixels, all pixels with 4-quadrant segmentation, and the SLIC representation with 4-quadrant partitioning. The results are shown in Tables 2, 3 and 4. Tables 2 and 3 show per class comparison. Table 4 compares overall performance.

Our approach shows the highest accuracy (82.5%) and the highest kappa value (76.84%). It also ranked as the highest or second highest for most classes (except grass) in user and producer accuracies. Qualitative analysis by visual comparison of the abundance and class maps with the color composite and reference data show that our results are closer to reference abundance maps and that the derived classification map better follows (than reference data) classes in the image (specially neighborhoods in in the left lower quadrant). Note that in the global approach, endmembers where poorly captured and their corresponding abundance maps are not as good as for the other cases. The regional full image unmixing using four tiles results in better results, which shows that regional unmixing identifies materials with a better accuracy. Regional unmixing with SLIC LD representation results in the best performance with additional computational gain and denoising from averaging.

4 Conclusions and Final Comments

The experimental results show that LD representation using superpixel segmentation provides an effective representation of the HSI for unmixing. Unmixing performance using the LD representations can result in equal or better performance than using the full image with denoising and computational gains. Also, regional segmentation results in improved performance for both the full and the LD dimensional representation.

Table 2: Producer's Accuracies for the 3 algorithms

	Asphalt Road	Grass	Trees	Roof	Dirt
Global	23.09%	**92.92%**	78%	82.94%	75.66%
4-tiles	72.98%	87.35%	70.31%	**89.89%**	86.11%
SLIC	**85.03%**	76.98%	**85.84%**	85.55%	**88.7%**

Table 3: User's Accuracies for the 3 algorithms.

	Asphalt Road	Grass	Trees	Roof	Dirt
Global	**99.86%**	87.79%	93.49%	**72.56%**	29.02%
4-tiles	91.1%	87.39%	**93.65%**	60.69%	**46.73%**
SLIC	95.72%	**97.08%**	85.33%	67.08%	45.14%

Table 4: Kohen's kappa and overall accuracies for the 3 algorithms.

	Kohen's Kappa	Overall Accuracy
Global	67.1%	76.34%
4-tiles	73.45%	80.36%
SLIC	**76.84%**	**82.5%**

5 References

[1] J. M. Bioucas-Dias, A. Plaza, N. Dobigeon, M. Parente, Qian Du, P. Gader, J. Chanussot, "Hyperspectral Unmixing Overview: Geometrical, Statistical, and Sparse Regression-Based Approaches," *IEEE J. Sel. Topics Appl. Earth Observe. in Remote Sens*. Vol. 5, No. 2, pp. 354-379, 2012.

[2] D.R. Thompson, L. Mandrake, M.S. Gilmore and R. Castaño, "Superpixel Endmember Detection," *IEEE Trans. Geosci. Remote Sens.* 48(11), 4023-4033, 2010.

[3] Saranathan, A.M. and Parente, M., "Uniformity-based Superpixel Segmentation of Hyperspectral Images," *IEEE Trans. Geosci. Remote Sens.* 54(3), 1419-1430, 2016.

[4] M. Goenaga-Jimenez and M. Velez-Reyes, "Integrating Spatial Information in Unmixing using the Nonnegative Matrix Factorization," *Proc. of SPIE*, Vol. 9088, 2014.

[5] M. Alkhatib and M. Velez-Reyes, "Understanding Spatial-Spectral Domain Interactions in Hyperspectral Unmixing using Exploratory Data Analysis," *Proc 8th IEEE WHISPERS*, August 21-24, 2016, Los Angeles, CA.

[6] R. Achanta, A. Shaji, K. Smith, A. Lucchi, P. Fua, and S. Susstrunk. *SLIC Superpixels*. Technical report, EPFL, 2010.

[7] M.A. Goenaga-Jimenez and M. Velez-Reyes, "Comparing Quadtree Region Partitioning Metrics for Hyperspectral Unmixing," *Proc. SPIE*, 8743, 1219- 1228, 2013.

[8] M. Aldeghlawi and M. Velez-Reyes, "Column Subset Selection Methods for Endmember Extraction in Hyperspectral Unmixing." *Proc. of SPIE*, Vol 10644, 2018.

[9] A. Kostrikin and Y. Manin, *Linear Algebra and Geometry*, Gordon and Breach Science Publishers, 1997.

[10] S. Rosario-Torres and M. Velez-Reyes, "An algorithm for fully constrained abundance estimation in hyperspectral unmixing." *Proc. of SPIE*, Vol. 5806, pp. 711-719, 2005.

[11] http://www.escience.cn/people/feiyunZHU/Dataset_GT.html

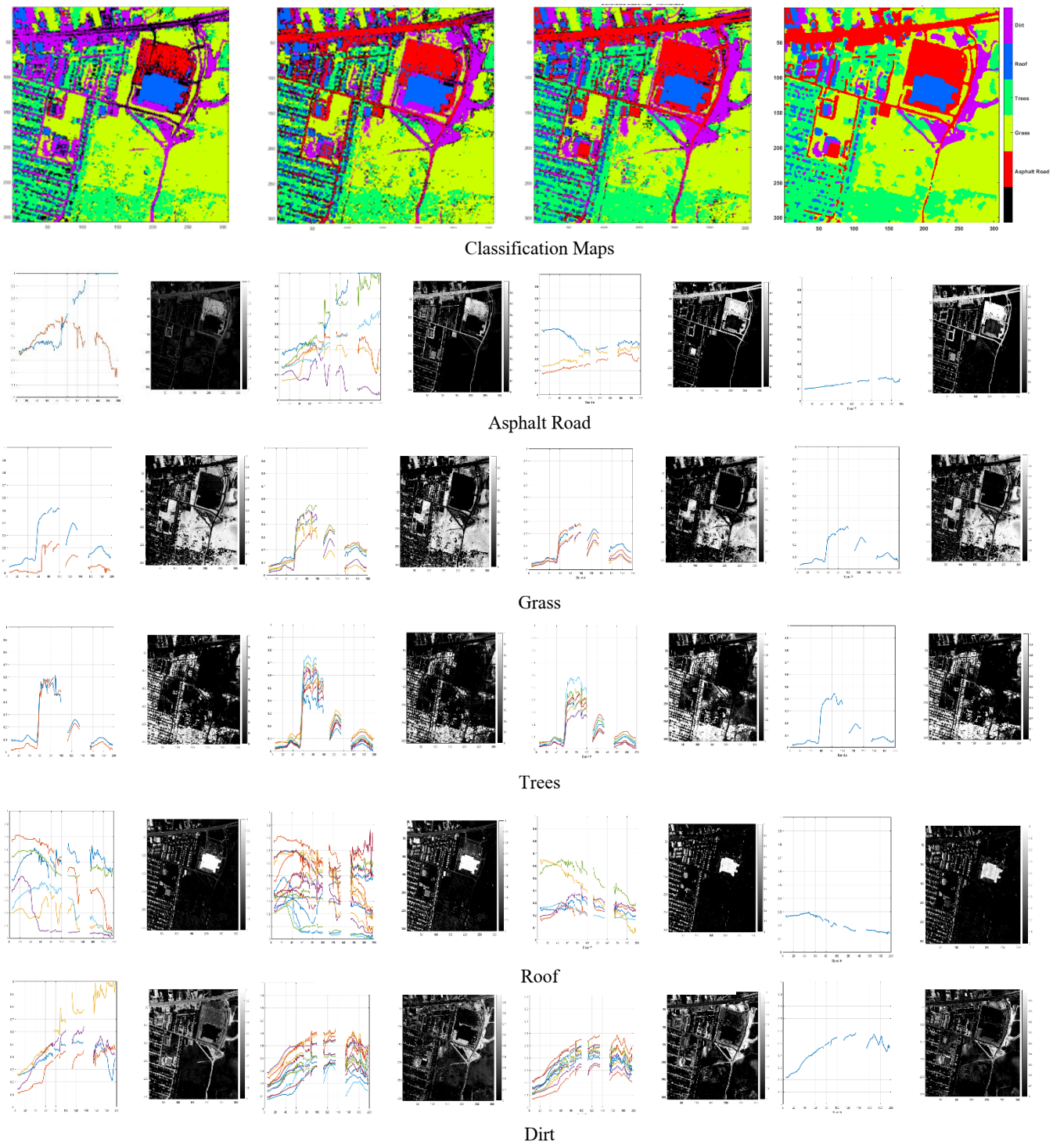

Fig. 4. Comparison of unmixing results between the proposed approach and other unmixing methods. Leftmost column shows the results of unmixing the full image (all pixels) using global unmixing. The second column shows the results for the full image with regional unmixing partitioning the image in 4 quadrants. The third column shows the results for the proposed SLIC-based regional unmixing. The fourth column (rightmost) shows the reference abundance maps from [11]. Note that unclassified pixels in the first row are shown in black.